Axial compressive behavior of laminated bamboo lumber columns with a chamfered section

Chaokun Hong[1a,1b,2], Haitao Li[1a,1b*], Zhenhua Xiong[3], Rodolfo Lorenzo[4], Xin Li[5], Zhen Wang[1a,1b]

[1a] College of Civil Engineering, Nanjing Forestry University, Nanjing 210037, China; [1b] Joint International Research Laboratory of Bio-composite Building Materials and Structures, Nanjing Forestry University, Nanjing 210037, China

[2] College of Civil Engineering and Architecture, Zhejiang University, Hangzhou 310058, China.

[3] Ganzhou Sentai bamboo company LTD, Ganzhou 341001, China.

[4] University College London, London WC1E 6BT, UK.

[5] School of Engineering, Deakin University, Geelong Waurn Ponds, VIC 3216, Australia.

*Corresponding author: Haitao LI, Professor, E-mail: lhaitao1982@126.com

Abstract: The axial compressive behavior of laminated bamboo lumber (LBL) columns with a chamfered section was investigated using 15 specimens with lengths varying from 600mm to 3000mm; all considered samples had same square cross section of 100 mm × 100 mm with 10 mm chamfers at each corner. Axial compression tests were carried out to analyze the impact of slenderness ratios on failure modes, strain and ultimate bearing capacity of LBL columns. Two failure modes were observed i.e. compression failure and buckling failure. Obtained results on the ultimate vertical strain and ultimate load showed a downward trend with the increase in slenderness ratios; the correlation between the ultimate strain, ultimate load and the slenderness ratios were fitted. The approximate solution method was adopted to reveal the lateral deflections of buckling columns by a quartic functional model. Based on the ideal elastic-plastic constitutive model and Hill failure criterion, FEM was carried out to simulate the axial compression tests. The simulation results agreed well with both test and theoretical results, which verified the feasibility of proposed methods used under similar working conditions in this paper.

Keywords: Laminated bamboo lumber; axial compression; buckling failure; approximate solution; finite element method

1 Introduction

Engineered bamboo is one of the bio-based building materials [1-6] including GluBam, parallel bamboo strand lumber (PBSL) and laminated bamboo lumber (LBL), which has a fast-growing characteristic (short forming time) with regular cross sections. Basic material properties and mechanical responses of these engineered bamboo products have been widely carried out [7-16] using experimental methods. Due to excellent physical and mechanical properties, they can be used in building structures. Compression is one of the most common force states in various types of building structures. The main force states when the column bears vertical load are axial compression [17] and eccentric compression [18], while transverse compression [19] and local compression [20] can be occurred when main and secondary beams overlap. Therefore, it is crucial to study the mechanical properties of structural members under compression for the safety design.

Research on the compressive properties and constitutive models of small LBL specimens have been carried out. Tinkler-Davies et al. [19] investigated the failure mechanism of LBL under

transverse compression using digital image correlation (DIC). Li et al. [21-22] revealed the compressive properties of LBL made from different growth parts of original bamboo (upper, middle, and lower parts). They found that the average compressive strength as well as the dispersion increased with the increase in growth positions, and proposed two-stage and three-stage constitutive models for LBL under parallel-to-grain compression. Sharma et al. [23] tested the basic material properties of PBSL (parallel bamboo strand lumber) and LBL, and reported that the mechanical properties of engineered bamboo were comparable to those of engineered timber. Yang et al. [24] investigated the off-axis compressive properties of LBL and verified the applicability of commonly used failure criteria. Based on the Ramberg-Osgood model [13], the constitutive models under compression at various texture angles were fitted. Wei et al. [25] studied the mechanical properties of LBL under axial compression, and proposed a compression constitutive model based on Richard Abbott model.

Research on the axial compressive properties of bamboo columns have also been carried out. Luna et al. [26] investigated the axial compressive properties of LBL columns with lengths varying from 150 mm to 2500 mm. Xiao et al. [27] carried out experimental research on the axial compressive properties of GluBam columns with lengths ranging from 401.8 mm to 1601.5 mm, and reported comparable results with 'GB 50005-2003 Code for design of timber structures' and 'American National Design Specification for Wood Construction'. Li et al. [28] tested the mechanical properties of LBL columns subjected to axial compression with the cross section of 100 mm × 100 mm and varying lengths between 400 mm and 1800 mm. They established an empirical formula of stability coefficient based on test data. Tian et al. [29] investigated the original bamboo columns and sprayed composite mortar–original bamboo composite columns with lengths varying from 500 mm to 3000 mm through axial compression tests, and proposed several methods for calculating relevant strength and stability capacities. Tan et al. [30] conducted research on the mechanical properties of PBSL columns with lengths between 400 mm and 1800 mm under axial compression, and compared the predicted ultimate load with Euler's equation, tangent modulus theory, double modulus theory and Newlin-Gahagan method.

Many attempts have been made to promote the use of engineered bamboo in construction. The earthquake-resistant bamboo villa [31], which was made from PBSL by Nanjing Forestry University, has a height of 3.2 m for the first floor and 2.8 m for the second floor; the bamboo house [32], which was built by Hunan University in Beijing Purple Bamboo Park, has 2 stories and a building height of 6.4 m; the office building, which was made from LBL and designed by Haitao Li's team and Ganzhou Sentai bamboo company LTD (Figure 1), has a building area of more than 1000 square meters with three stories and a building height of 12.7 m. It is foreseeable that engineered bamboo will gain more attention from the construction industry.

Figure 1 LBL office building (reproduced with permission of Haitao Li)

Despite of existing practical applications, the design as well as construction methods for engineered bamboo house are normally following experience or referring to timber structures. That is, there is lack of standardization and pertinence for the time being. In recent years, although increasing number of studies on engineered bamboo were carried out by researchers, the test results are still far from enough to develop a unified design code [31]. Most of the experimental studies were carried out based on columns below 2 m, and therefore, existing empirical equations proposed to calculate ultimate bearing capacity are insufficient as practical columns are normally higher than 2 m. The deformation control of structural members is important in design as well. However, compared with stub columns, the actual lateral deflections are hard to measure in long column as a result of buckling failure due to unpredictable deflection direction and suddenly failure mechanism. In the existing studies, the actual lateral deflections of the buckling columns may be neglected.

In summary, there is lack of research on axial compression behavior of large-scale LBL columns (over 2m) and actual lateral deflections of buckling columns. Therefore, current paper considered slenderness ratios as impact factor and conducted axial compression tests for LBL columns with lengths varying from 600 mm to 3000 mm, a cross section of 100 mm × 100 mm, and 10 mm chamfers at each corner. Furthermore, approximate solutions for lateral deflections of buckling columns were obtained, and finite element analyses were carried out to perform comparable studies.

2 Experimental programs

2.1 Materials

Laminated bamboo lumber used for testing were produced by Ganzhou Sentai bamboo company LTD in Jiangxi Province, China. Moso bamboo (from Yongan, Fujian) and resorcinol adhesive were used as raw materials, and bamboo strips (7 mm × 21 mm × 2005 mm) were hot-pressed together under the pressure of 9 MPa for upper and lower surface and 6.5 MPa for the left and right surface in 157 ℃ conditions for about 15 minutes. The arrangement of bamboo strips and the cross section of the laminated bamboo columns are shown in Figure 2. To meet the length requirements in the longitudinal direction, mechanical connection was applied to single bamboo strips (Figure 3). The moisture content and density of the specimen were 7.0% and 736 kg/m³, respectively.
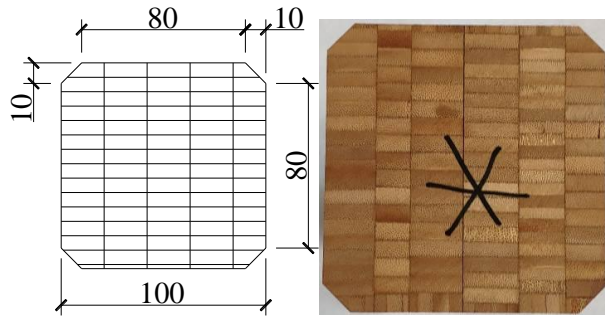
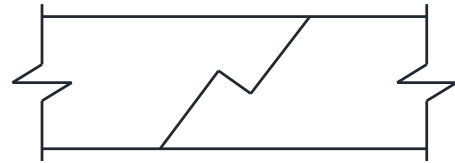Figure 2 Arrangement of bamboo strips and cross section of laminated bamboo column

Figure 3 Mechanical connection

A total number of 15 LBL columns (5 groups, 3 replicates for each group) were designed according to the length i.e. 600 mm, 1100 mm, 1700 mm, 2300 mm and 3000 mm, as shown in Figure 4. They are related to slenderness ratios of 21.14, 38.75, 59.89, 81.02 and 105.68, respectively. Square cross section of 100 mm × 100 mm with four 10 mm chamfers at relevant corners of the section was selected as shown in Figure 2. All the columns took the wide surface of the bamboo strip as side A, and marked the remaining wide surfaces as side B, C and D successively along the counterclockwise direction. The top surface was marked with ＊, while the bottom surface left blank.

Figure 4 Specimens with different slenderness ratios
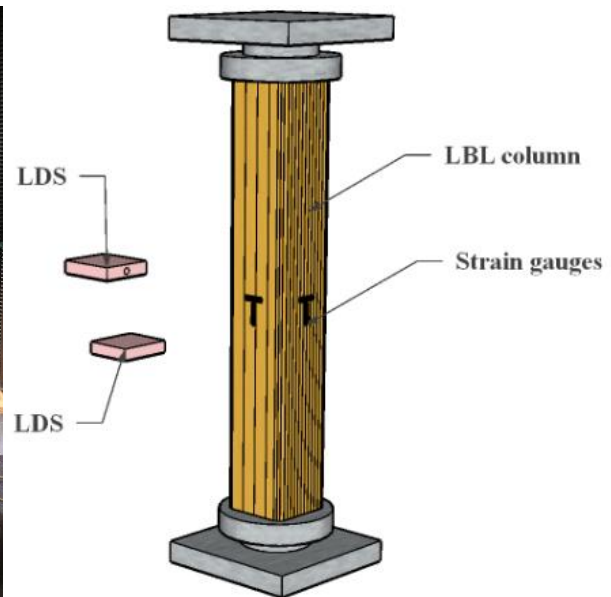
Figure 5 Test setup

Figure 6 Schematic diagram

2.2 Test arrangement and measurements

Test setup was designed according to the standard for test methods of timber structures (GB/T 50329-2012) as shown in Figure 5 and Figure 6. Two spherical hinge supports were used to ensure that the specimen could rotate freely in any direction. Ropes were loosely set on the specimens to avoid hazards when column buckling occurred. Test data was collected through a TDS-540 data acquisition instrument. Load was applied by using a microcomputer-controlled electro-hydraulic servo universal testing machine (100 t). The axial displacement of the specimen was measured by

a displacement meter, whilst the lateral deflection of two adjacent surfaces at the middle height of the column were measured by two additional laser displacement sensors. Besides, lateral and vertical strain gauges were applied at the mid-height of the four side surfaces to observe the change of strain with the load.

The geometric alignments were considered for positioning samples ensuring the geometric center of the column is in line with the center of the testing machine. Five preloading cycles were implemented prior to test until the vertical strains of the four sides were close to each other, which could ensure that the specimen was in the state of axial force. All samples were tested in the structure laboratory at Nanjing Forestry University with controlled testing time within 10 minutes for each sample.

3 Test results and discussion

3.1 Failure modes

In the axial compression test, the failure modes of the LBL columns can be mainly divided into two types, namely compression failure and buckling failure.

Compression failure was specifically defined when the end of the specimen was crushed or partially buckled, as shown in Figure 7 (A600-3 as an example). An initial linear elastic state in specimen up to 80%~90% of the ultimate load was observed followed by a slowly increase in load showing the initial of yield. At this stage, the cracking sound inside the specimen could be heard. The upper end of the specimen began bending, and then cracks occurred at the corner of the section. As the load further increased to the ultimate load, the cracks rapidly expanded to the middle of the specimen, and the upper end of the column crushed gradually with multi-cracks. Applied load slowly reduced once exceed the maximum carrying capacity, but the specimen was still able to bear certain load before the specimen suddenly broke and lost its carrying capacity. Figure 7b~7g shows each side surface of A600-3 after unloading.

（a）Compression process of A600-3

(b) Side A   (c) Side B   (d) Side C   (e) Side D   （g）Bottom surface
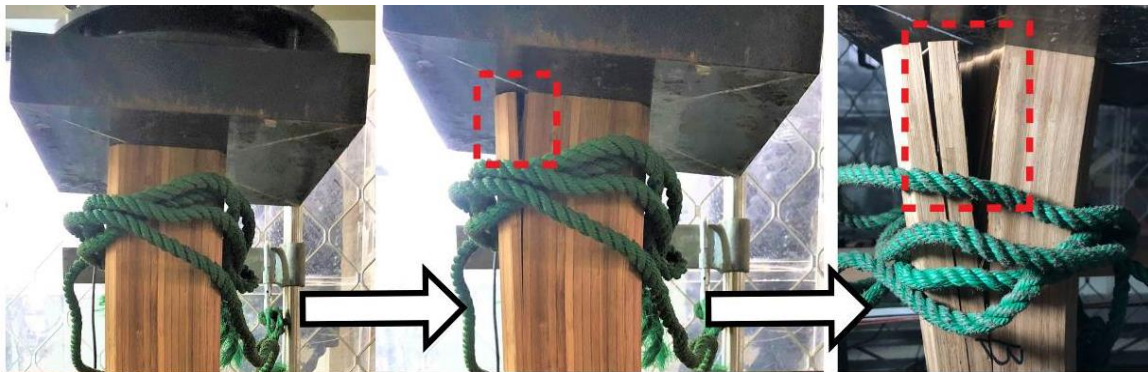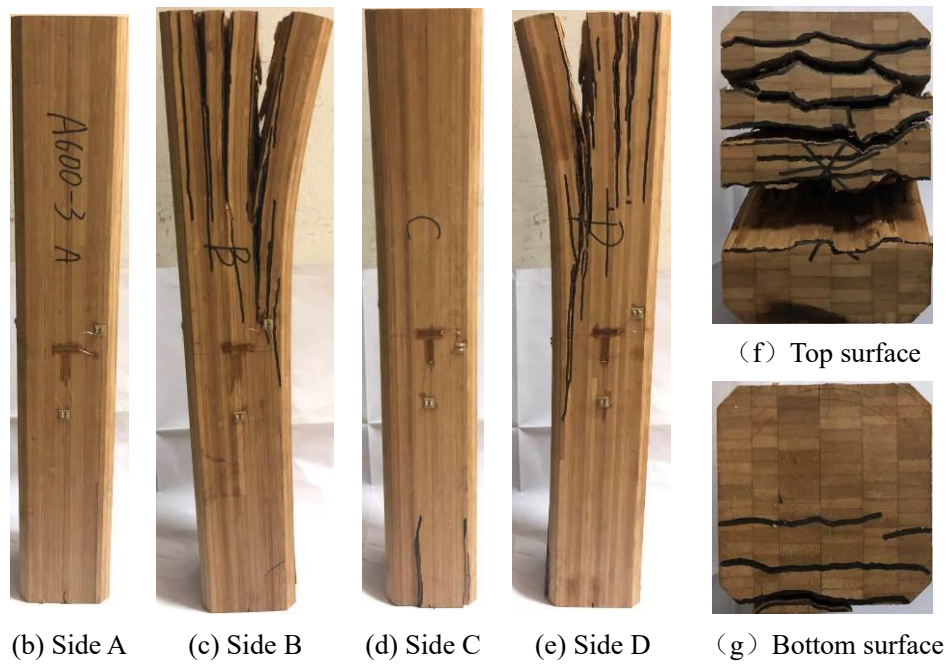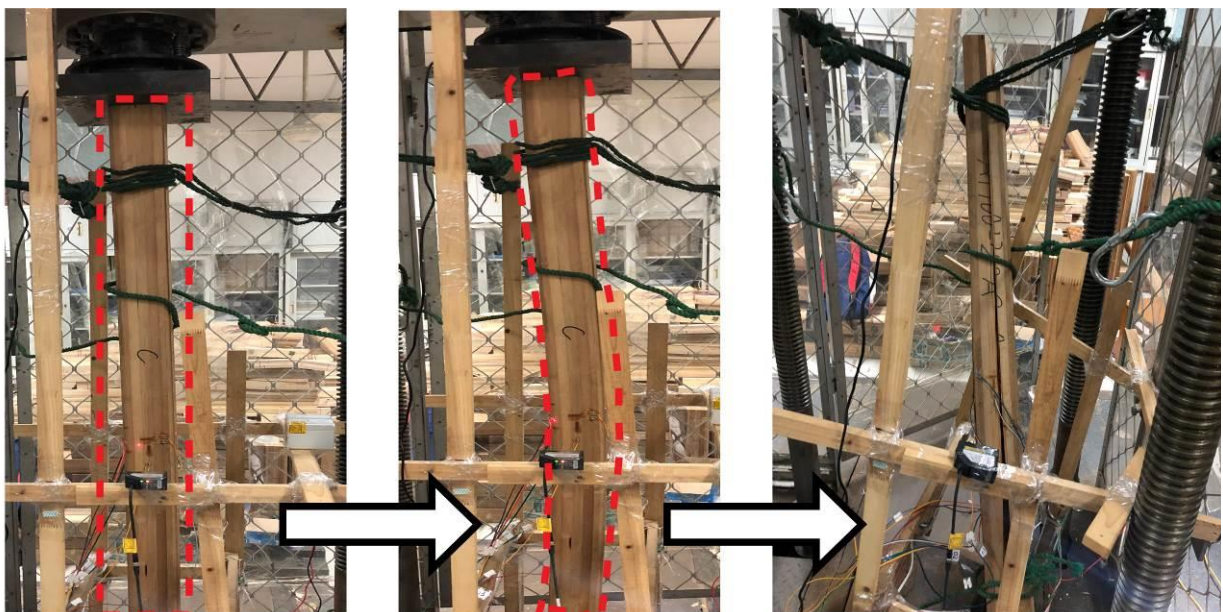
Figure 7 Compression process and failure phenomena of A600-3

With the increase in slenderness ratios, the initial defects of the columns, such as manufacturing errors and initial bending, showed a more significant impact on the bearing capacity. As shown in Figure 8a (A1700-2 as an example), although similar phenomenon to short columns during initially loading when the load increased to 80% ~ 90% of the ultimate load, the deflection change rate at the mid-height gradually accelerated in longer samples, while a relatively large bending deformation was observed. At the end of loading, the specimen buckled and ejected from the loading machine. Specimens with buckling failure mode failed in a more drastic manner when compared with specimens with compression failure mode. Figure 8b shows the A~D side surfaces of A1700-2. It is worth noting that no crack was occurred during loading process, but observed cracks were caused by the collision between the column and protective net after buckling.

（a）Compression process of A1700-2

（b）Failure phenomena of A1700-2

Figure 8 Compression process and failure phenomena of A1700-2

3.2 Main test results

The main test results are shown in Table 1, where P_{max} is the ultimate load, f_c is the compressive strength, ε_{ua} and ε_{ul} are the average ultimate strain of four side surfaces in the vertical and lateral direction, respectively. Except for the ultimate strain, all other test data showed relevant coefficient of variation (COV) less than 20% indicating reliable results obtained from current setup. Larger COVs (exceeds 20%) of the ultimate strain values were observed for Group A600 and A1100. It is due to the fact that the specimen cracked before reaching the ultimate load so that the surface was in an unloaded manner resulting in a decrease value of the average ultimate strain. Load-displacement curves for A1100 samples showed a plastic stage during loading but the compressive strain eventually converted to tensile strain, and therefore, they are classified as buckling failures.

Table 1 Main test results

Group	P_{max} /kN	S_{ul} /mm	f_c /MPa	ε_{ua} / $\mu\varepsilon$	ε_{ul} / $\mu\varepsilon$	E /MPa	Failure Mode
A600-1	411.53	7.30	41.99	8675	2787	8176	
A600-2	586.94	15.05	59.89	20914	5927	8632	
A600-3	464.16	7.39	47.36	8603	2976	9020	Compression failure
Mean	487.54	9.92	49.75	12731	3897	8609	
COV	15%	37%	15%	45%	37%	4%	
A1100-1	447.83	12.16	45.70	10005	3621	8892	Buckling failure, but existing phenomenon of compression failure
A1100-2	385.25	6.11	39.31	4923	1375	8804	
A1100-3	495.08	15.72	50.52	11964	3228	8516	
Mean	442.72	11.3	45.18	8964	2741	8737	
COV	10%	35%	10%	33%	36%	2%	
A1700-1	383.57	10.72	39.14	5755	1856	8625	
A1700-2	373.56	9.02	38.12	5346	1577	8764	Buckling failure
A1700-3	359.60	8.84	36.69	5034	1482	8776	
Mean	372.24	9.53	37.98	5378	1639	8722	

Group	P_{max} /kN	S_{ul} /mm	f_c /MPa	ε_{ua} / $\mu\varepsilon$	ε_{ul} / $\mu\varepsilon$	E /MPa	Failure Mode
COV	3%	9%	3%	5%	10%	1%	
A2300-1	301.33	8.78	30.75	3603.50	955.00	8941	
A2300-2	286.58	8.67	29.24	3521.00	941.75	8286	
A2300-3	299.46	8.62	30.56	3582.75	1202.25	9199	Buckling failure
Mean	295.79	8.69	30.18	3569.08	1033.00	8809	
COV	2%	1%	2%	1%	12%	4%	
A3000-1	225.91	8.84	23.05	2592.50	712.25	8955	
A3000-2	212.83	8.06	21.72	2512.50	715.00	8776	
A3000-3	—	—	—	—	—	—	Buckling failure
Mean	219.37	8.45	22.38	2552.50	713.63	8866	
COV	3%	5%	3%	2%	0%	1%	

Note: The test of A3000-3 was terminated due to unforeseen technical issues.

3.3 Load-deflection behaviors

Load-deflection behaviors for specimens with different slenderness ratios are shown in Figure 9. At the initial stage of loading, the laminated bamboo column was uniformly compressed in the axial direction with no obvious lateral deflection observed in the middle of the specimen. When the load increased to 80% ~ 90% of the ultimate load, the increasing rate of mid-span deflection gradually accelerated, and obvious deflection could be observed at this stage. After reaching the ultimate load, the reaction force in the compression failure group stably decreased, while that in the buckling failure group basically maintained. Due to the limitation of the test site, the mid-span deflection values of A2300 and A3000 were not measured in this test.

It is worth noting that the bending direction of the column cannot be predicted because the initial defects of the specimen were not able to be quantified. During the test, it was found that the bending direction of some specimens was not strictly toward the two laser displacement sensors. Figure 9 only plots the larger data which cannot accurately show the real deflection at the middle of the specimen. In Table 2, the measured mid-span deflection of Surface A and B, and the distance from the outermost surface to the initial axis position are shown. The results showed that the actual lateral deflection increased with the increase in slenderness ratio.
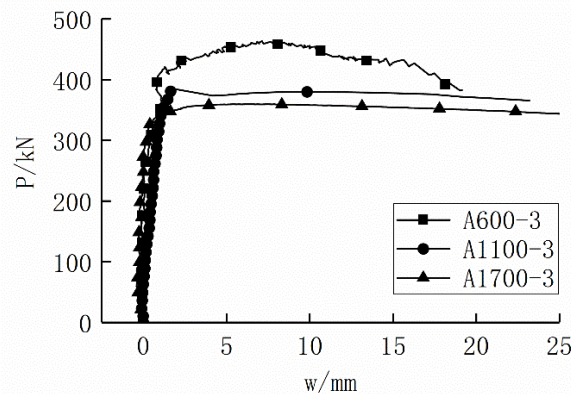

Figure 9 Load vs deflection curves

Table 2 Deflection values of Surface A and Surface B

Group	Surface A (mm)	Surface B (mm)	Distance from Z axis (mm)	Mean
A600-1	7.81	2.35	77.99	77.31
A600-2	—	—	—	
A600-3	7.85	0.26	76.63	
A1100-1	1.43	12.00	80.55	77.38
A1100-2	0.05	1.77	72.00	
A1100-3	6.34	6.22	79.59	
A1700-1	14.71	2.21	83.15	78.91
A1700-2	4.52	6.54	78.54	
A1700-3	0.25	5.73	75.04	

Note: Data of A600-2 was lost due to the failure of laser displacement sensor. Distance from Z axis refers to the distance from the outermost surface at the mid-height to the initial axis of the column at the moment of reaching the ultimate load, $Z = \sqrt{(A+50)^2 + (B+50)^2}$.

3.4 Load-displacement behaviors

Figure 10 shows the load-displacement curves for specimens with different slenderness ratios. Curves for short columns exhibited an obvious yield stage prior to failure. However, buckling columns showed two types of deform pattern. On the one hand, a certain but shorter yield stage compared to short columns could be observed before reaching failure, such as A1100 series. On the other hand, curves without obvious yield stage during the loading process was observed showing a brittle descent stage, which indicated that most part of the laminated bamboo column might still be within the linear elastic stage before the final failure, i.e. the stress under the ultimate load did not exceed the proportional limit of laminated bamboo material. In general, obtained ultimate load, ultimate axial displacement and stiffness of the specimen decreased with the increase in slenderness ratios.
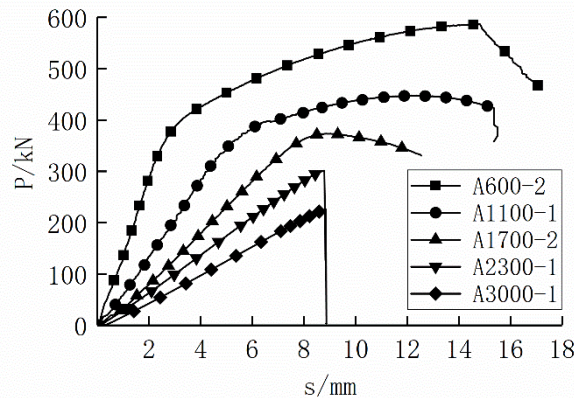

Figure 10 Load vs axial displacement curves

3.5 Load-strain behaviors

Figure 11 shows the load-strain behaviors for specimens with different slenderness ratios. As shown in Figure 10 (a), all surfaces for compression failure samples were subjected to

compressive strains; the column exhibited an elastoplastic state during the loading process. Initial linear load-strain curves followed by a yield stage with gradually decreased slope until reaching the ultimate load.

As shown in Figure 11(b)~(e), surfaces for buckling failure samples were subjected to compressive strain but some of them decreased before the final failure; the section of slender column was uniformly compressed at the initial stage showing approximately linear load-strain curves. With the increase in load, lateral deflection gradually appeared in column, and the vertical strain in one or two surfaces began to deviate when compared with other surfaces. When the load increased to about 80% to 90% of the ultimate load, the compressive strain on the deviated surfaces gradually decreased, and even converted to a tensile strain. When the load reached the peak, the compressive strain on other surfaces rapidly increased, and so did the deflection degree of the column.

(a) A600-2

(b) A1100-1

(c) A1700-3

(d) A2300-1
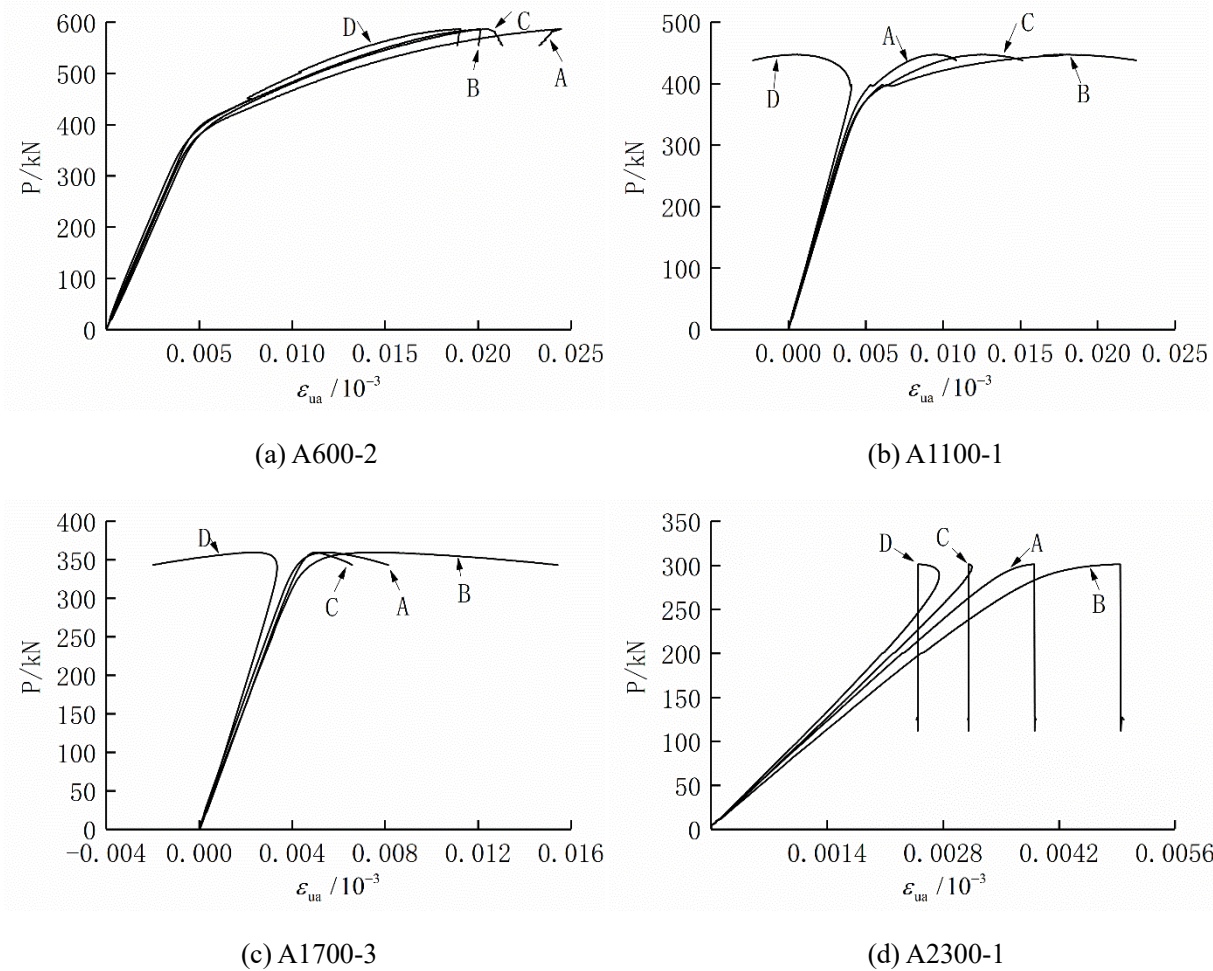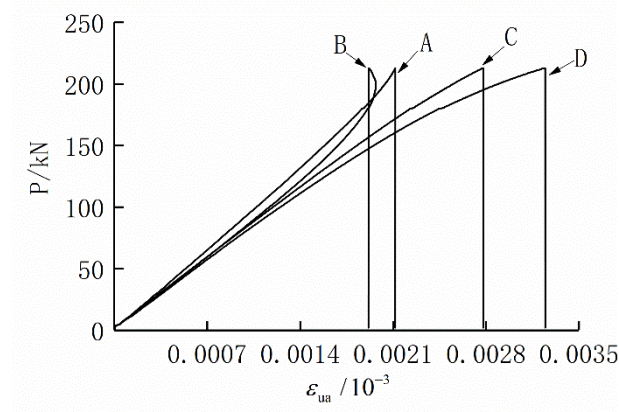
(e) A3000-1

Figure 11 Load vs vertical strain curves

3.6 Relationship between ultimate strain, ultimate load and slenderness ratio

The formulas for calculating the slenderness ratio of the column are given as Equations (1) and (2):

$$\lambda = l_0 / i \tag{1}$$

$$i = \sqrt{I / A} \tag{2}$$

where l_0 is the calculated length of the column; i is the section radius of gyration; I is the section moment of inertia; A is the section area. The moment of inertia I (Figure 12) can be calculated using Equation (3).
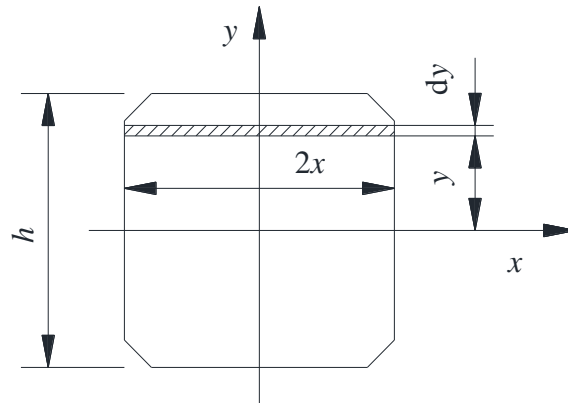

Figure 12 Moment of inertia of the column section

$$I_x = \int_A y^2 dA = 2\int_{40}^{\frac{h}{2}} y^2 \times 2x dy + 2\int_0^{40} y^2 \times 2x dy = 4\int_{40}^{50} y^2 (90 - y) dy + 4\int_0^{40} y^2 \times 50 dy \tag{3}$$
$$= 7.9 \times 10^6 \, mm^4$$

Figure 13 (a) and (b) shows the relationship between the vertical ultimate strain, lateral ultimate strain and slenderness ratio, respectively, where the ultimate strain is the mean value of each group. Significantly higher vertical and lateral ultimate strain were obtained for compression failed specimen indicating better use of material properties when compared with buckling failed specimen. Furthermore, the ultimate strain showed a downward trend with the increase in slenderness ratio.
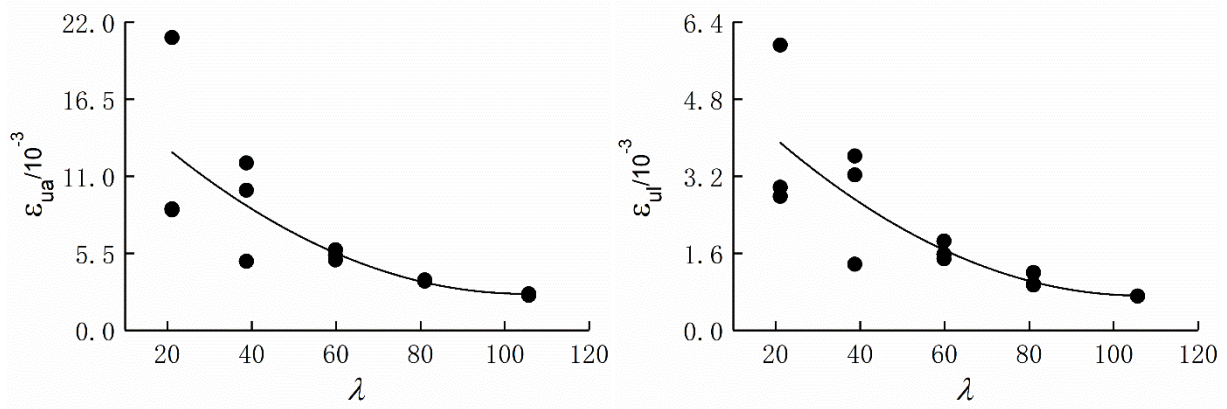
(a) Ultimate vertical strain   (b) Ultimate lateral strain

Figure 13 Relationship between the ultimate strain and slenderness ratio

By using regression analysis, the relationship between the ultimate strain and the slenderness ratio can be described by Equations (4) and (5):

$$\varepsilon_{ua} = 1.4464\lambda^2 - 303.07\lambda + 18489 \tag{4}$$

$$\varepsilon_{ul} = 0.4357\lambda^2 - 92.817\lambda + 5667.2 \tag{5}$$

where ε_{ua} is the vertical ultimate strain of the mid-height, ε_{ul} is the lateral ultimate strain; λ is the slenderness ratio.

Figure 14 shows the relationship between the ultimate load and the slenderness ratio of the specimen, where ultimate load decreased approximately linearly with the increase in slenderness ratio.
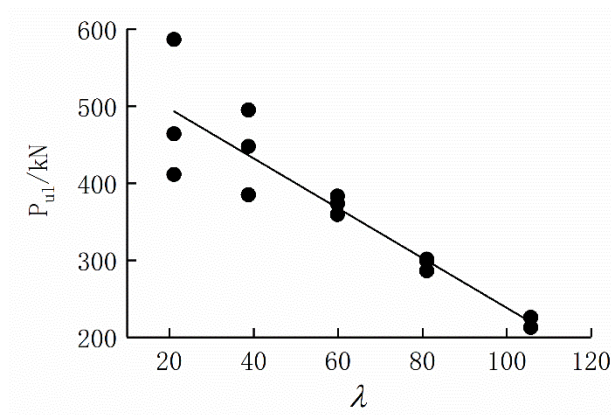

Figure 14 Relationship between the ultimate load and slenderness ratio

By using regression analysis, the relationship between the ultimate strain and the slenderness ratio can be described by Equation (6):

$$P_{ul} = -3.24\lambda + 561.93 \tag{6}$$

where P_{ul} is the ultimate load, λ is the slenderness ratio.

3.7 Comparison of ultimate bearing capacity formulas

Some scholars have carried out experimental research on the mechanical properties of square section bamboo columns under axial compression, and established the ultimate bearing capacity formulas based on the test data. To verify the feasibility of these existing formulas, calculated results are listed in Table 3 and are compared with obtained test results in current study. Meanwhile, the design codes for timber structures in terms of bearing capacity of axially compressed columns are also evaluated for comparison.

The critical buckling load obtained by Euler's equation is:

$$P = \frac{n^2 \pi^2 EI}{L^2} \tag{7}$$

where P is the critical load for a column, n is the mode of buckling, E is the modulus of elasticity, I is the second moment of area, and L is the effective length for the pinned-pinned boundary conditions.

Li et al. [28] proposed Equation (8) to calculate the ultimate bearing capacity of the laminated bamboo column:

$$N_{ul} = \varphi f_c A = (0.000106 (l_0 / h)^2 - 0.0298 (l_0 / h) + 1.1) f_c A \tag{8}$$

where N_{ul} is the ultimate load, φ is the stability coefficient, f_c is the compression strength of the laminated bamboo, A is the area of the cross section, l_0 is the effective length of the laminated bamboo column and h is the height of the cross section.

Tan et al. [30] proposed Equation (9) to calculate the ultimate capacity of parallel strand bamboo column:

$$P = 0.098 \lambda^2 - 12.87 \lambda + 842.47 \tag{9}$$

where P is the ultimate load, λ is the slenderness ratio.

In the design standard of timber structure GB 5005-2017, the stability coefficient of axially compressed members can be calculated according to different materials and wood species. For wood species with strength grade of TC17, TC15 or TB20, it can be expressed as:

$$\varphi = \frac{1}{1 + (\lambda / 80)^2}, \lambda \leq 75 \tag{10}$$

For wood species with strength grade of TC11, TC13, TB11, TB13, TB15 or TB17, it can be expressed as:

$$\varphi = \frac{1}{1 + (\lambda / 65)^2}, \lambda \leq 91 \tag{11}$$

where φ is the stability coefficient, λ is the slenderness ratio.

In the National Design Specification for Wood Construction NDS-2018, the stability coefficient C_p of axially compressed members can be calculated by Equation (12~16):

$$C_{\mathrm{p}} = \frac{1+\left(F_{\mathrm{cE}}/F_{\mathrm{c}}^*\right)}{2c} - \sqrt{\left[\frac{1+\left(F_{\mathrm{cE}}/F_{\mathrm{c}}^*\right)}{2c}\right]^2 - \frac{F_{\mathrm{cE}}/F_{\mathrm{c}}^*}{c}} \tag{12}$$

$$F_{\mathrm{cE}} = \frac{0.822E_{\mathrm{min}}'}{\left(l_{\mathrm{e}}/d\right)^2} \tag{13}$$

$$l_{\mathrm{e}} = k_1 l \tag{14}$$

if the allowable stress method is adopted, E_{min}' and F_{c}^* may be determined using Equation (15) and (16):

$$E_{\mathrm{min}}' = \frac{1.05\left(1-1.645COV_{\mathrm{E}}\right)E}{1.66} \tag{15}$$

$$F_{\mathrm{c}}^* = F_{\mathrm{c}} \times C_{\mathrm{D}} \times C_{\mathrm{M}} \times C_{\mathrm{t}} \times C_{\mathrm{i}} \times C_{\mathrm{F}} \tag{16}$$

where F_{c}^* is the design value of compressive strength in the parallel-to-grain direction. F_{cE} is the nominal Euler yield strength. c is the coefficient related to the material, and 0.9 for Glulam. k_1 is the effective length factor, which is taken as 1.0 according to the boundary conditions. l is the length of the column and l_{e} is the effective length. d is the section width. E is the elastic modulus and E_{min}' is the elastic modulus used to calculate the stability of column. COV_{E} is the coefficient of variation of elastic modulus, and the value is taken as 0.1. C_{D} is the load duration factor, which is conservatively taken as 1.0. C_{M} is the wet service factor, which should be taken as 0.73 for calculating the design value of compressive strength when the environmental humidity is higher than 16%. C_{t} is the temperature factor, which should be taken as 1.0 for testing at room temperature (20 °C). C_{i} is the incising factor, which should be taken as 0.8 for calculating the bearing capacity. C_{F} is the size factor, which is conservatively taken as 1.0.

Tan et al. [33] also proposed a modified strength reduction factor for LBL material based on same functional model like Equation (12), which can be expressed as:

$$\phi_{mLB} = \begin{cases} 0.8 * \left(\dfrac{1.4+\left(F_{\mathrm{cE}}/F_{\mathrm{c}}^*\right)}{2c} - \sqrt{\left[\dfrac{1.4+\left(F_{\mathrm{cE}}/F_{\mathrm{c}}^*\right)}{2c}\right]^2 - \dfrac{\left(F_{\mathrm{cE}}/F_{\mathrm{c}}^*\right)+0.4}{c}} \right) & \dfrac{F_{\mathrm{cE}}}{F_{\mathrm{c}}^*} \leq 1 \\[3em] 0.75 * \left(\dfrac{1.4+\left(F_{\mathrm{cE}}/F_{\mathrm{c}}^*\right)}{2c} - \sqrt{\left[\dfrac{1.4+\left(F_{\mathrm{cE}}/F_{\mathrm{c}}^*\right)}{2c}\right]^2 - \dfrac{\left(F_{\mathrm{cE}}/F_{\mathrm{c}}^*\right)+0.4}{c}} \right) & \dfrac{F_{\mathrm{cE}}}{F_{\mathrm{c}}^*} > 1 \end{cases} \tag{17}$$

where ϕ_{mLB} is the modified strength reduction factor.

The predicted values of ultimate bearing capacity calculated by Euler's equation showed a large deviation from the real value with relative errors ranged between 27.11% and 282.31%, as shown in Table 3. Results obtained from Li et al.'s equation [28] seemed to be more reliable when

compared with Tan et al.'s equation [30], as same engineered bamboo with close dimensions of the specimen were used. However, relative error for A3000 was 19.71%, which is still large for empirical equation. It may be caused by the fact that the fitted equation did not include the data of long columns, and also, the variable h in Equation (8) is not suitable for samples with chamfers in current study. The functional model of Equation (9) seemed to be inappropriate for this study as the calculated values for A2300 and A3000 were larger than short columns, which was not impossible. Results obtained from Tan et al.'s new equation [33] were conservative with relative errors ranged between 2.06% and 17.95%, whereas the functional model was much more reliable than before.

Predicted values from GB 5005-2017 equation showed relatively agreement with the test values. Smaller errors within 12.04% were obtained for wood species with strength grade of TC17, TC15 and TB20. Predicted values from NDS-2018 equation for A600 and A1100 agreed well with the experimental values with errors less than 14.47%. However, for the specimens longer than 1700 mm, predicted values were too conservative to fully use the materials. For now, the stability coefficient of TC17 etc. may be suitable for the design of laminated bamboo columns, whereas for short columns are inappropriate.

Therefore, a more suitable functional model should be chosen along with large numbers of tests on columns with various lengths should be conducted in the future to develop a unified design code for laminated bamboo columns.

Table 3 Compared results of different formulas

Group	A600/kN	A1100/kN	A1700/kN	A2300/kN	A3000/kN
Test results	487.54	442.72	372.24	295.79	219.37
Euler's equation	1863.78	562.76	235.21	129.78	76.78
Error	282.28%	27.11%	36.81%	56.12%	65%
Li et al. [28]	540.56	458.75	364.67	275.05	176.13
Error	10.87%	3.62%	2.03%	7.01%	19.71%
Tan et al. [30]	614.19	490.91	423.19	443.04	576.86
Error	25.98%	10.89%	13.69%	49.78%	162.96%
TC17 etc.	546.24	473.32	374.50	288.47	212.87
Error	12.04%	6.91%	0.61%	2.48%	2.96%
TC11 etc.	528.49	431.14	316.07	228.82	160.38
Error	8.40%	2.62%	15.09%	22.64%	26.89%
NDS-2018	558.09	419.56	208.45	118.38	70.84
Error	14.47%	5.23%	44%	59.98%	67.71%
Tan et al. [33]	421.54	394.58	305.44	253.92	223.88
Error	13.54%	10.87%	17.95%	14.16%	2.06%

Note: The compressive strength used for calculation was 59.63 MPa. $\text{Error} = \left| \text{Calculation} - \text{test} \right| / \text{test} \times 100\%$.

4 Numerical studies

4.1 Approximate solution method for buckling columns

Under ideal conditions, the lateral deflection in axially loaded members with hinged supports

at both ends follows a sine half-wave function curve, on which Euler derived the critical force formula. However, test observations indicated that the lateral deflection in LBL column did not follow a sine half-wave curve. This might be caused by the difference between actual boundary conditions and ideal conditions resulting in bending moments at both ends of the column. Therefore, in many studies, the predictive ultimate load calculated by Euler's equation deviated largely from the test values. According to Section 3.3, the deflection direction in some specimens was oblique which was not strictly towards the position of the two laser displacement sensors. Thus, Figure 9 cannot accurately represent the real deflection of the middle part of the specimens. To obtain the deflection curve equation at the time of column buckling and to further obtain the maximum deformation value in the middle span, an approximate solution method was adopted to solve this problem.
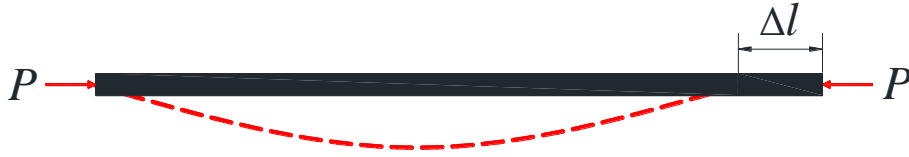
Figure 15 Axial compression

LBL column was simplified to a thin pole (Figure 15) and conformed to the assumption of 'plane sections remain plane'. The length of the column can be indicated by a deflection curve w:

$$l = \int_0^{l-\Delta l} \sqrt{1 + \left(\frac{\mathrm{d}w}{\mathrm{d}x}\right)^2}\,\mathrm{d}x \approx \int_0^{l-\Delta l}\left[1 + \frac{1}{2}\left(\frac{\mathrm{d}w}{\mathrm{d}x}\right)^2\right]\mathrm{d}x \approx l - \Delta l + \int_0^l \frac{1}{2}\left(\frac{\mathrm{d}w}{\mathrm{d}x}\right)^2 \mathrm{d}x \tag{18}$$

Therefore, the axial shortening value of the columns Δl is expressed as:

$$\Delta l = \int_0^l \frac{1}{2}\left(\frac{\mathrm{d}w}{\mathrm{d}x}\right)^2 \mathrm{d}x \tag{19}$$

By defining Rayleigh quotient [34]:

$$R = \frac{\dfrac{1}{2}\int_0^l EI\left(\dfrac{\mathrm{d}^2 w}{\mathrm{d}x^2}\right)^2 \mathrm{d}x}{\dfrac{1}{2}\int_0^l \left(\dfrac{\mathrm{d}w}{\mathrm{d}x}\right)^2 \mathrm{d}x} \tag{20}$$

where the molecule is the bending strain energy of the rod and the denominator is the axial shortening value. The stationary point of Rayleigh quotient is the critical load at which the geometric possible displacement corresponds to the buckling mode, i.e.

$$P_{cr} = \mathrm{st}\frac{\int_0^l EI\left(\dfrac{\mathrm{d}^2 w}{\mathrm{d}x^2}\right)^2 \mathrm{d}x}{\int_0^l \left(\dfrac{\mathrm{d}w}{\mathrm{d}x}\right)^2 \mathrm{d}x} \tag{21}$$

To take the extreme value of the quotient of Equation (21) and let it be zero:

$$\delta \int_0^l EI \left(\frac{d^2 w}{dx^2} \right)^2 dx - P\delta \int_0^l EI \left(\frac{dw}{dx} \right)^2 dx = 0 \qquad (22)$$

The two integral terms of Equation (22) are calculated by variational operation:

$$\int_0^l \left[\frac{d^2}{dx^2} \left(EI \frac{d^2 w}{dx^2} \right) + P \frac{d^2 w}{dx^2} \right] \delta w dx - \left\{ \left[\frac{d}{dx} \left(EI \frac{d^2 w}{dx^2} \right) + P \frac{dw}{dx} \right] \delta w \right\}_0^l + \left[EI \frac{d^2 w}{dx^2} \delta \left(\frac{dw}{dx} \right) \right]_0^l = 0 \; (23)$$

The governing equation can then be obtained:

$$\frac{d^2}{dx^2} \left(EI \frac{d^2 w}{dx^2} \right) + P \frac{d^2 w}{dx^2} = 0 \qquad (24)$$

Boundary conditions:

$$\begin{cases} w = 0 \; \text{or} \; \dfrac{d}{dx} \left(EI \dfrac{d^2 w}{dx^2} \right) + P \dfrac{dw}{dx} = 0 \\[4mm] \dfrac{dw}{dx} \; \text{or} \; EI \dfrac{d^2 w}{dx^2} = 0 \end{cases} \qquad (25)$$

Let the trial function w be a quartic function:

$$w = \frac{x}{l} \left(1 - \frac{x}{l} \right) \left[a_1 + a_2 \frac{x}{l} \left(1 - \frac{x}{l} \right) \right] \qquad (26)$$

where w is the lateral deflection of the column; l is the length of the column; a_1 and a_2 are undetermined parameter. w approximately satisfies the boundary condition. According to Equation (26), the equations for axial shortening value and bending strain energy can be obtained as follows:
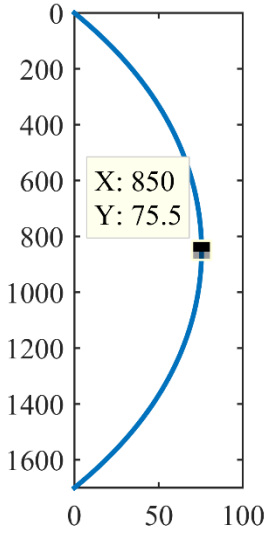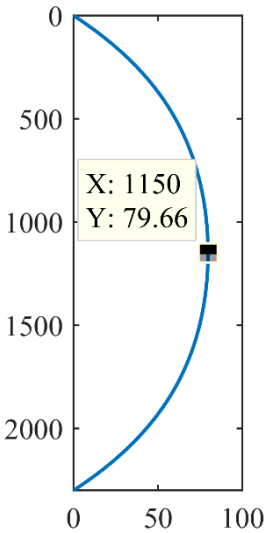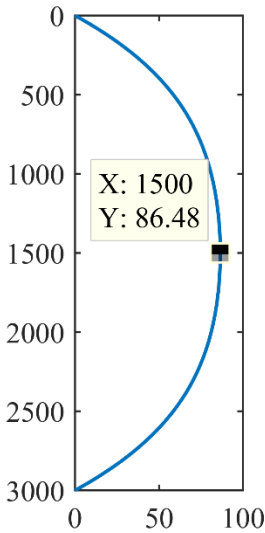
$$\frac{1}{2} \int_0^l \left(\frac{dw}{dx} \right)^2 dx = \frac{35a_1^2 + 14a_1 a_2 + 2a_2^2}{210l} \qquad (27)$$

$$\frac{1}{2} \int_0^l EI \left(\frac{d^2 w}{dx^2} \right)^2 dx = \frac{2EI(5a_1^2 + a_2^2)}{5l^3} \qquad (28)$$

By introducing the axial shortening value and ultimate load, the undetermined parameter a_1 and a_2 can be obtained by substituting test values into Equation (20), (27) and (28). For A600 and A1100 groups with compression failure mode, a large part of the axial shortening was due to volume deformation that caused by compression, so there is no solution or only a complex-number solution. For A1700 ~ A3000 groups, there were four pairs of real solutions, and only the first-order solution was retained in this paper (Table 4). It can be seen that the relative error between measured value and calculated value for A1700 was 4.32%, which verified the correctness of the approximate solution method to a certain content. The trend i.e. the lateral deflections increased with the increase in slenderness ratio obtained by theoretical results was consistent with the measured results in Section 3.3. To further validate aforementioned observations, a 3D finite

element model (FEM) was developed in the Section 4.2.

Table 4 Approximate solution

Group	A1700	A2300	A3000
Calculated deflection curves at ultimate load	X: 850 Y: 75.5	X: 1150 Y: 79.66	X: 1500 Y: 86.48
First-order solution	$a_1 = 346.56\ a_2 = -178.31$ or $a_1 = -346.56\ a_2 = 178.31$	$a_1 = 431.49\ a_2 = -451.37$ or $a_1 = -431.49\ a_2 = 451.37$	$a_1 = 515.27\ a_2 = -677.43$ or $a_1 = -515.27\ a_2 = 677.43$
Measured Distance from Z axis (mean value)	78.91mm	—	—
Calculated distance from Z axis	75.5mm (4.32%)	79.66mm	86.48mm

Note: Due to the limitation of the test site, the mid-span deflection values of A2300 and A3000 were not measured in this test. $\text{Error} = |\text{Calculation} - \text{test}| / \text{test} \times 100\%$

4.2 Finite element analysis

To further verify the rationality of the approximate solution method, based on ABAQUS explicit dynamic analysis method, the finite element method was adopted for comparative analyses.

4.2.1 Hill failure criterion

Referring to the research by Jasieńko et al. [35] and Tang et al. [36], Hill failure criterion [37] was selected for strength analysis. The Hill failure criterion is expressed as:

$$F(\sigma_{ij}) = \sqrt{\frac{F(\sigma_{22} - \sigma_{33})^2 + G(\sigma_{33} - \sigma_{11})^2 + H(\sigma_{11} - \sigma_{22})^2}{+2L\sigma_{23}^2 + 2M\sigma_{31}^2 + 2N\sigma_{12}^2}} < \sigma_0 \tag{29}$$

where σ_{ii} is the normal stress; σ_{ij} is the shear stress; F, G, H, L, M and N are constant values determined by material properties and can be calculated by Equations (30) ~ (35):

$$F = \frac{(\sigma_0)^2}{2}\left(\frac{1}{\bar{\sigma}_{22}^2} + \frac{1}{\bar{\sigma}_{33}^2} - \frac{1}{\bar{\sigma}_{11}^2}\right) = \frac{1}{2}\left(\frac{1}{R_{22}^2} + \frac{1}{R_{33}^2} - \frac{1}{R_{11}^2}\right) \tag{30}$$

$$G = \frac{(\sigma_0)^2}{2}\left(\frac{1}{\bar{\sigma}_{33}^2} + \frac{1}{\bar{\sigma}_{11}^2} - \frac{1}{\bar{\sigma}_{22}^2}\right) = \frac{1}{2}\left(\frac{1}{R_{33}^2} + \frac{1}{R_{11}^2} - \frac{1}{R_{22}^2}\right) \tag{31}$$

$$H = \frac{(\sigma_0)^2}{2}\left(\frac{1}{\bar{\sigma}_{11}^2} + \frac{1}{\bar{\sigma}_{22}^2} - \frac{1}{\bar{\sigma}_{33}^2}\right) = \frac{1}{2}\left(\frac{1}{R_{11}^2} + \frac{1}{R_{22}^2} - \frac{1}{R_{33}^2}\right) \tag{32}$$

$$L = \frac{1}{2}\left(\frac{\tau_0}{\bar{\sigma}_{23}^2}\right)^2 = \frac{3}{2R_{23}^2} \tag{33}$$

$$M = \frac{1}{2}\left(\frac{\tau_0}{\bar{\sigma}_{13}^2}\right)^2 = \frac{3}{2R_{13}^2} \tag{34}$$

$$N = \frac{1}{2}\left(\frac{\tau_0}{\bar{\sigma}_{12}^2}\right)^2 = \frac{3}{2R_{12}^2} \tag{35}$$

where $\bar{\sigma}_{ii}$ is the strength of material in three directions; $\bar{\sigma}_{ij}$ is the shear strength of material;

σ_0 is a reference value used to determine material failure, $\tau_0 = \frac{\sigma_0}{\sqrt{3}}$. R_{ij} can be calculated by

Equation (36):

$$R_{11} = \frac{\bar{\sigma}_{11}}{\sigma_0}, R_{22} = \frac{\bar{\sigma}_{22}}{\sigma_0}, R_{33} = \frac{\bar{\sigma}_{33}}{\sigma_0}, R_{12} = \frac{\bar{\sigma}_{12}}{\tau_0}, R_{13} = \frac{\bar{\sigma}_{13}}{\tau_0}, R_{23} = \frac{\bar{\sigma}_{23}}{\tau_0} \tag{36}$$

4.2.2 Constitutive model and finite element model

Constitutive models and compressive strength of small LBL specimens are described in the Introduction part, however, most of the studies only reflect mechanical properties in the parallel-to-grain direction. Laminated bamboo lumber is a typical anisotropic material, even it could be simplified as an orthotropic material in finite element analyses, the difference of ultimate strength, elastic modulus and Poisson's ratio in three directions should be considered.

The ideal elastic-plastic constitutive model of LBL used is shown in Figure 16, where X_t and X_c are the tensile strength and compressive strength of LBL along the grain direction (L), Y_t and Y_c are the tensile strength and compressive strength along the radial direction (R), Z_t and Z_c are the tensile strength and compressive strength along the tangential direction (T), respectively.
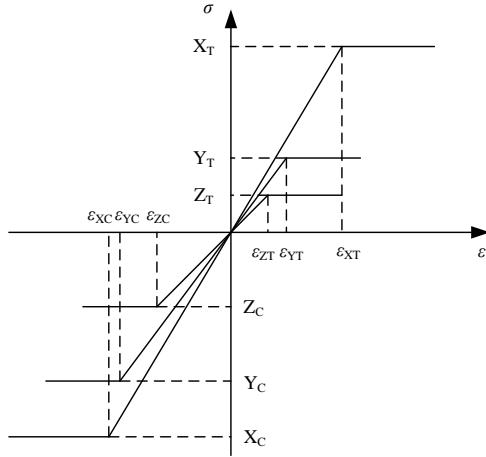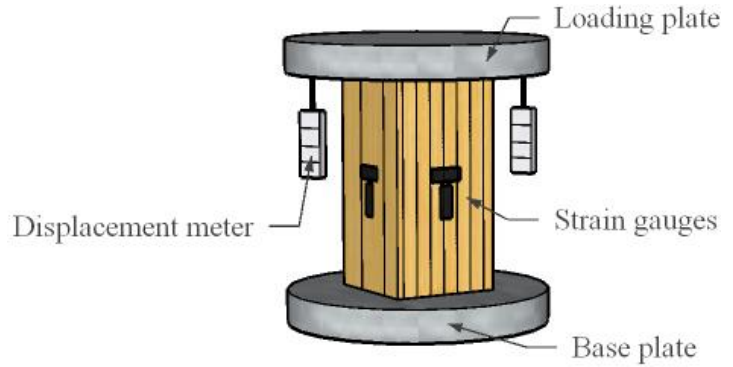
Figure 16 Constitute model

Figure 17 Material test

To obtain effective and reliable parameters for constitutive model i.e. compressive strength, elastic modulus and Poisson's ratio in three directions, basic materials from the same batch were used to fabricate 36 longitudinal specimens, 36 radial specimens and 36 tangential specimens with dimensions of 50mm×50mm×100mm for compression tests (Figure 17). The main test results are shown in Table 5. The shear properties of LBL were referred to the research by Saliklis et al. [38] and Ramirez et al. [39] with shear modulus, elastic modulus and Poisson's ratio expressed as Equations (37). Shear strengths of S_{XY}, S_{YZ} and S_{ZX} were used same as Tang et al. [36].

$$G_{TL} = \frac{\sqrt{E_L E_T}}{2(1+\sqrt{\mu_{TL}\mu_{LT}})}, \quad G_{RT} = \frac{\sqrt{E_R E_T}}{2(1+\sqrt{\mu_{RT}\mu_{TR}})}, \quad G_{RL} = \frac{\sqrt{E_R E_L}}{2(1+\sqrt{\mu_{RL}\mu_{LR}})} \quad (37)$$

Table 5 Constitutive model parameters

Modulus (MPa)		Poisson's ratio		Strength (MPa)			
E1	6323.70	μ12	0.25	X_T	98	S_{XY}	18.13
E2	1468.53	μ21	0.054	Xc	59.63	S_{YZ}	22.59
E3	1192.06	μ13	0.2	Y_T	8.26	S_{ZX}	6.58
G12	1365.08	μ31	0.04	Y_C	21.91	σ_0	59.63
G23	461.81	μ23	0.43	Z_T	8.26		
G13	1260.09	μ32	0.435	Z_C	19.85		

Figure 18 shows the finite element model of A600. Same FE model technique was adopted to other sample groups. The element type of Explicit/C3D8R and a meshing density of 10 (approximate global size) were implemented. The surfaces at both ends of the specimen were coupled at two reference points at the center of the section. The boundary conditions were set at the reference point, and the degree of freedom U1, U2 and U3 were restricted according to the test conditions. To meet the requirements of quasi-static analysis with the kinetic energy less than 10% of the strain energy, the calculation time was set to 1s. The displacement loading was carried out by using smoothing analysis step.
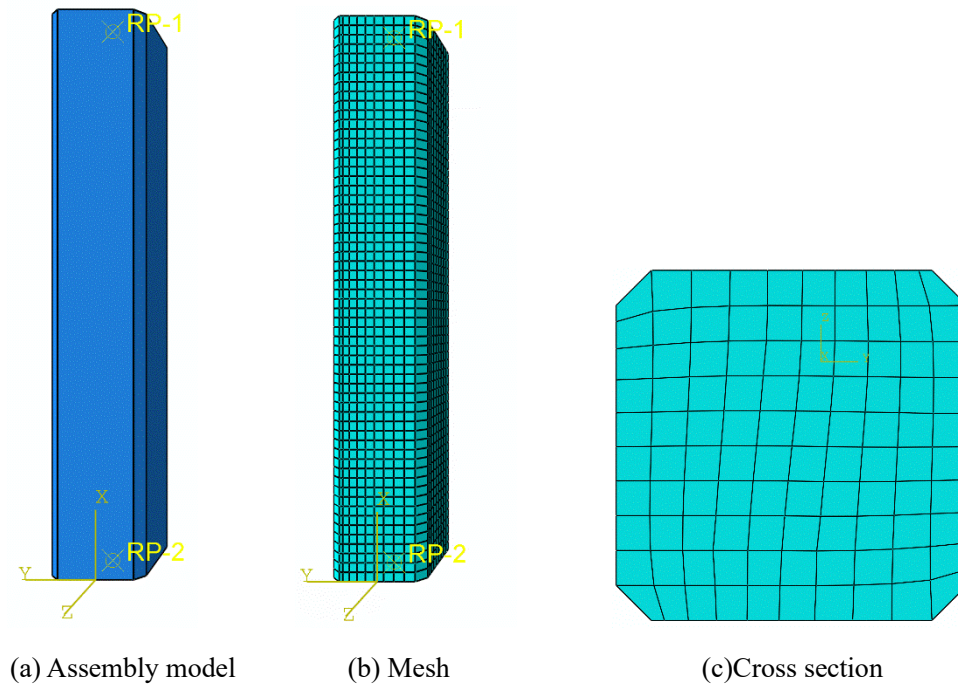
| (a) Assembly model | (b) Mesh | (c)Cross section |

Figure 18 Finite element model

4.2.3 Simulation results and analysis

Figure 19 plots the load-axial displacement curves and the stress clouds of the specimens corresponding to the ultimate load moment. The stress cloud for A600 showed that the whole section of specimen reached the maximum stress of 59.63 MPa when compression failure occurred. However, unlike A600, the maximum stress area of the specimen was not uniformly distributed along the column when buckling failure occurred indicating oblique deflections involved. The simulation results matched well with the experimental phenomenon, which confirmed the rationality of proposed finite element model.

For specimens with length of 1700mm, relative error between the ultimate bearing capacity obtained by simulation and the test was larger than 20%. The reason is that the failure mode in shorter specimens were compression failure where the ultimate load mainly depended on the compressive strength of the material along the grain direction, however, in longer specimens, buckling failure may occurred and the ultimate load became more sensitive to the elastic modulus along the grain direction. The elastic modulus parallel to grain was 6323.7MPa in simulation, which was quite different from the actually measured i.e. 8749MPa (A600-A3000 average value); therefore, obtained results from FE were very conservative. For analysis of A1700 ~ A3000 groups, the elastic modulus along the grain direction was adjusted to 8749MPa to consider this concern, and better results were obtained as expected.

Table 6 compares the results between the simulation and test. Analysis from Figure 19 and Table 5 indicated that the shape of the load-axial displacement curves matched the test curves and the relative error between the simulated ultimate load and the test value was within 20%. It confirmed that the simulation of LBL columns using ideal elastic-plastic constitutive model and Hill failure criterion was effective and feasible. Nevertheless, this model cannot perfectly reflect

the plastic stage of the specimens, i.e., the ductility of the structure. Table 6 also shows the simulation results including the mid-span deflections and the distance from Z-axis. For buckling columns under the working conditions in this paper, obtained relative error was within 3.34% showing good agreements between FE and the first-order approximate solution, which proved the rationality of the approximate solution method. For shorter A600 and A1100 groups, the measured and simulated values of the distance from Z-axis were partly larger than those of buckling failure specimens. The reason is that specimens with compression failure showed certain ductility resulted in larger deformation during loading.
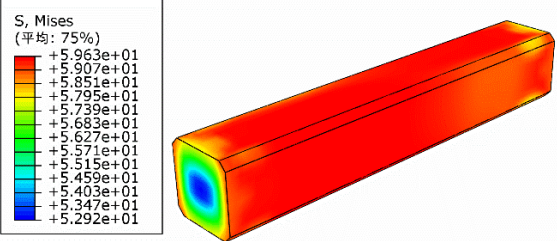
(a) Stress cloud of A600 at 585.70kN
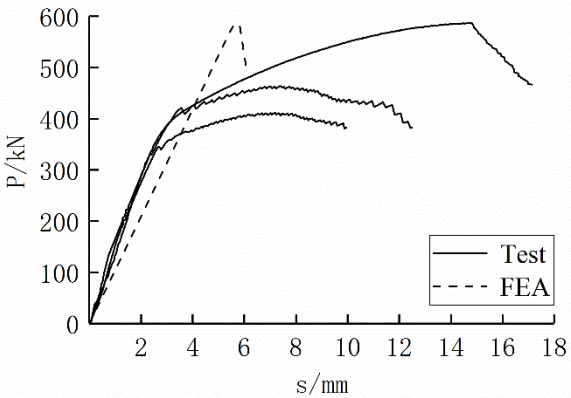
(b) A600 load-displacement curves
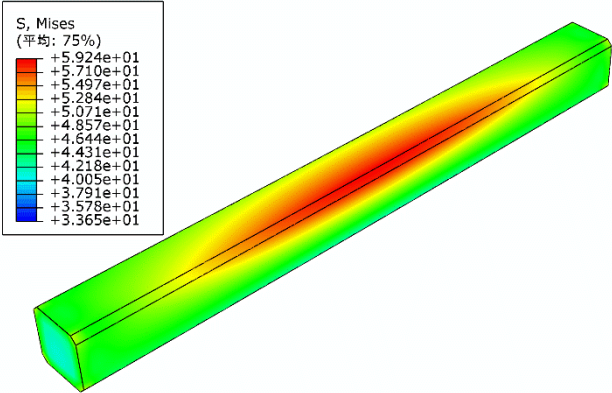
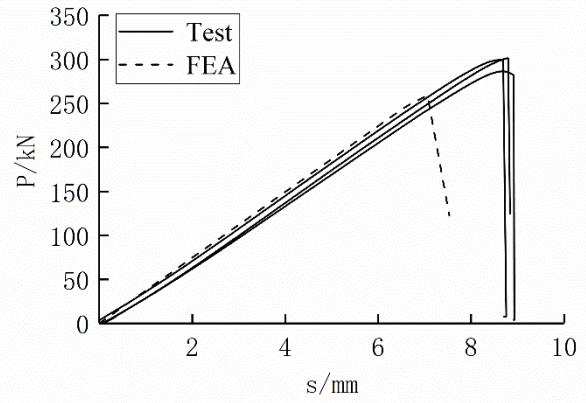(c) Stress cloud of A1100 at 456.35kN
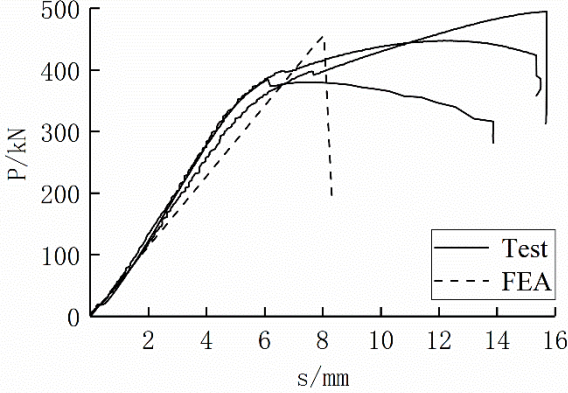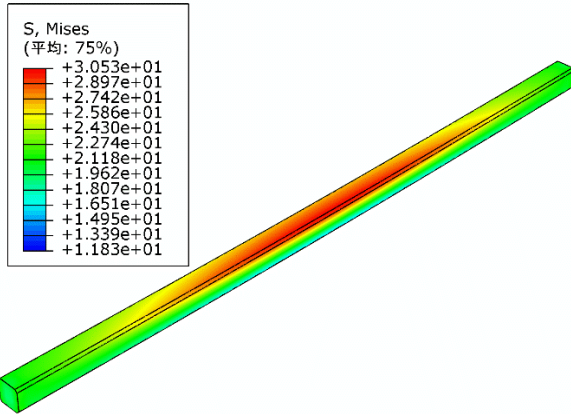

(d) A1100 load-displacement curves
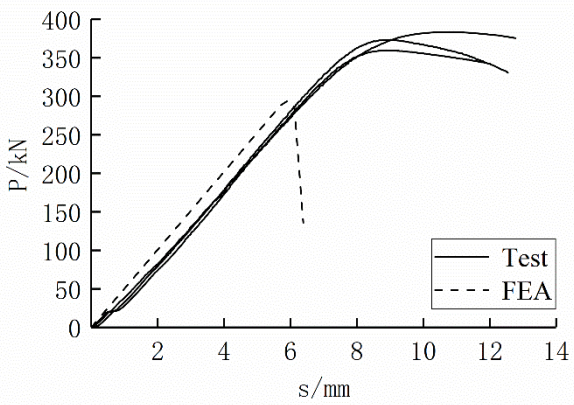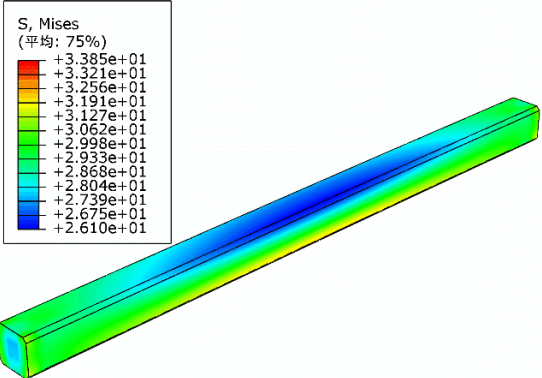
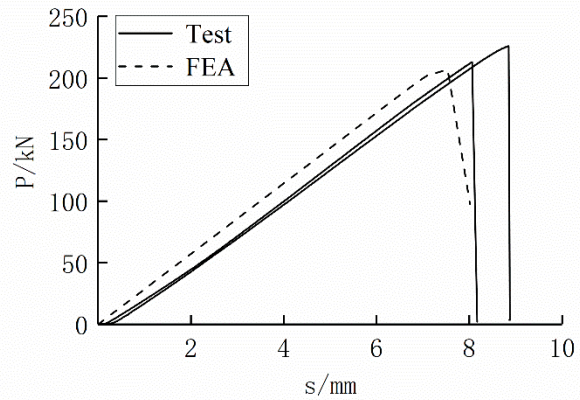(e) Stress cloud of A1700 at 294.64kN　　　　　　　(f) A1700 load-displacement curves
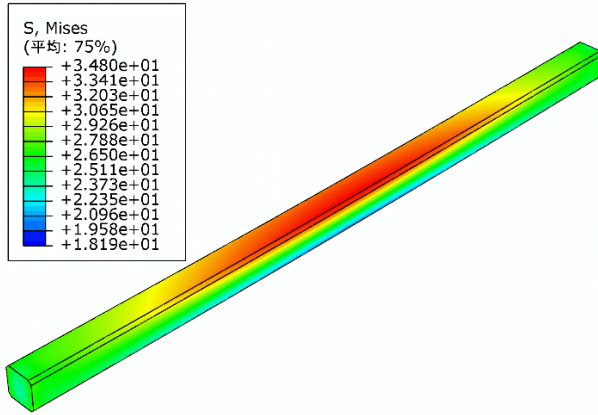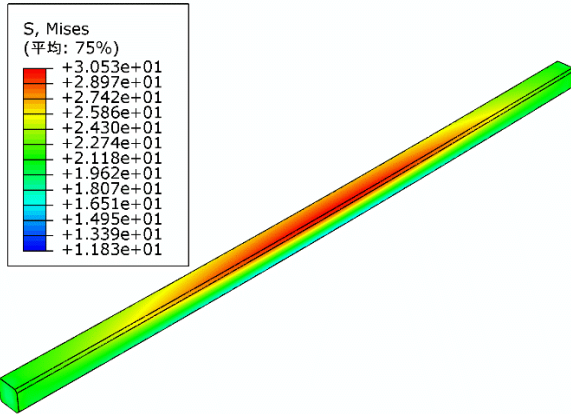

(g) Stress cloud of A2300 at 259.12kN　　　　　　　(h) A2300 load-displacement curves

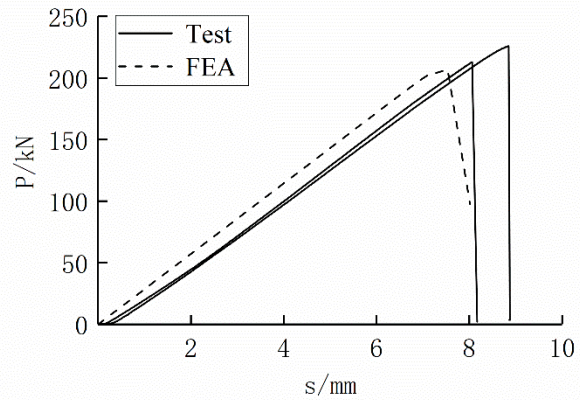(i) Stress cloud of A3000 at 206.8kN　　　　　　　　(j) A3000 load-displacement curves

Figure 19 Stress cloud and load-displacement curves

Table 6 Compared results

Group	P_{FEA}/kN	P_{ul}/kN	Error1	Surface A/mm	Surface B/mm	Distance from Z axis/mm	First-order solution/mm	Error2
A600	585.70	487.54	20.13%	0.01	0.1	70.79	—	—
A1100	456.35	442.72	3.08%	1.95	4.00	74.93	—	—
A1700	294.64	372.24	20.85%	0.55	2.64	72.98	75.5	3.34%
A2300	259.12	295.79	12.40%	1.12	10.92	79.53	79.66	0.16%
A3000	206.80	219.37	6.06%	4.11	19.03	87.71	86.48	1.42%

Note: P_{FEA} is the simulated ultimate load; P_{ul} is the test result; $Error1 = \left| P_{FEA} - P_{ul} \right| / P_{ul} \times 100\%$; $Error2 = \left| \text{Distance from Z axis} - \text{First-order solution} \right| / \text{First-order solution} \times 100\%$.

5 Conclusions

In this paper, compression tests considering the slenderness ratios as influencing factor were carried out on laminated bamboo columns to study the axial compressive behavior and lateral deflections. The approximate solution method and finite element method were adopted to analyze with following conclusions summarized as:

(1) The failure modes of the LBL columns could be mainly divided into two types, namely

compression failure and buckling failure. For specimens with compression failure, all four sides were subjected to compressive strains. However, for specimens with buckling failure, variations in strain values on some surfaces were observed close to failure i.e. decreased or even converted to tensile strain.

(2) With the increase in slenderness ratios, the influence of initial imperfection on the deformation and bearing capacity of specimens became significant gradually, and the ultimate strain and ultimate load showed a downward trend. The relationship between ultimate strain, ultimate load and slenderness ratios were fitted and could be expressed by quadratic function and linear function, respectively. Meanwhile, calculated bearing capacity from existing literature were compared and discussed indicating the requirement of further investigations on LBL columns with practical lengths to form a unified design code in the future.

(3) For long columns suffering from buckling failures, the lateral deflections at the ultimate load could be obtained by using a quartic function that approximately satisfied the boundary conditions. Theoretical results showed that the lateral deflections increased with the increase in slenderness ratios. The measured lateral deflection value for A1700 specimen was in good agreement with the calculated value, which verified the correctness of the approximate solution method to a certain extent.

(4) Based on the ideal elastic-plastic constitutive model and Hill failure criterion, axial compression tests were simulated for comparative analysis. Obtained distribution of stress clouds in models were consistent with the experimental phenomena, and relative errors of ultimate bearing capacity between test values and simulation values were less than 20% basically. The 3D finite element model developed in this study can be used to calculate the ultimate bearing capacity of LBL columns, whereas it cannot perfectly reflect the deformation of short columns subjected to compressive failure.

(5) To further verify the correctness of the approximate solution method, theoretical lateral deflections of buckling columns were compared with simulation results. Obtained relative errors were within 3.34%, which verified the feasibility of the approximate solution method under the working conditions considered in current study.

The authors declare that they have no conflicts of interest to this work.

References:

[1] Sun XF, He MJ, Li Z. Novel engineered wood and bamboo composites for structural applications: State-of-art of manufacturing technology and mechanical performance evaluation. Construction and Building Materials 2020; 249: 118751. https://doi.org/10.1016/j.conbuildmat.2020.118751.

[2] Li HT, Xuan YW, Xu B, et al. Bamboo application in civil engineering field. Journal of Forestry Engineering 2020; 5(6): 1-10. DOI: 10.13360/j.issn.2096-1359.202003001.

[3] Wang X, Zhou A, Zhao L, et al. Mechanical properties of wood columns with rectangular hollow cross section. Construction and Building Materials 2019; 214: 133-142. https://doi.org/10.1016/j.conbuildmat.2019.04.119.

[4] Lou ZC, Yang LT, Zhang AW, et al. Influence of saturated steam heat treatment on the bamboo color. Journal of Forestry Engineering 2020; 5(4): 38-44. DOI: 10.13360/j.issn.2096-1359.201906044.

[5] Wei X, Chen FM, Wang G. Flexibility characterization of bamboo slivers through winding-based bending stiffenss method. Journal of Forestry Engineering 2020; 5(2): 48-53. DOI: 10.13360/j.issn.2096-1359.201905046.

[6] Lou ZC, Yuan CL, Li YJ, et al. Effect of saturated steam treatment on the chemical composition and crystallinity properties of bamboo bundles. Journal of Forestry Engineering 2020; 5(2): 29-35. DOI: 10.13360/j.issn.2096-1359.201905014.

[7] Mahdavi M, Clouston PL, Arwade SR. Development of Laminated Bamboo Lumber: Review of Processing, Performance, and Economical Considerations. J Mater Civ Eng 2011; 23:1036–42. https://doi.org/10.1061/(asce)mt.1943-5533.0000253.

[8] Lv Q, Ding Y, Liu Y. Study of the bond behaviour between basalt fibre-reinforced polymer bar/sheet and bamboo engineering materials. Advances in Structural Engineering 2019; 22(14): 3121-3133. https://doi.org/10.1177/1369433219858725.

[9] Sun LW, Bian YL, Zhou AP, et al. Study on short-term creep property of bamboo scrimber. Journal of Forestry Engineering 2020; 5(2): 69-75. DOI: 10.13360/j.issn.2096-1359.201905021.

[10] Zhong Y, Ren H Q, Jiang Z H. Effects of temperature on the compressive strength parallel to the grain of bamboo scrimbe. Materials 2016; 9(6): 436. https://doi.org/10.3390/ma9060436.

[11] Wei Y, Zhou M Q, Chen D J. Flexural behaviour of glulam bamboo beams reinforced with near-surface mounted steel bars. Materials Research Innovations 2015; 19(sup1): S1-98-S1-103. https://doi.org/10.1179/1432891715Z.0000000001377.

[12] Chen G, Jiang H, Yu Y, et al. Experimental analysis of nailed LBL-to-LBL connections loaded parallel to grain. Materials and Structures 2020; 53(4): 1-13. https://doi.org/10.1617/s11527-020-01517-5.

[13] Qiu ZY, Fan HL. Nonlinear modeling of bamboo fiber reinforced composite materials. Compos Struct 2020;238:111976. https://doi.org/10.1016/j.compstruct.2020.111976.

[14] Chen G, Yu Y, Li X, He B. Mechanical behavior of laminated bamboo lumber for structural application: an experimental investigation. Eur J Wood Wood Prod 2020;78:53–63. https://doi.org/10.1007/s00107-019-01486-9.

[15] Li X, Ashraf M, Li HT, Zheng X, Al-Deen S, Wang H, et al. Experimental study on the deformation and of parallel bamboo Strand Lumber under drop-weight penetration impact. Constr Build Mater 2020;242:118135. https://doi.org/10.1016/j.conbuildmat.2020.118135.

[16] Leng Y, Xu Q, Harries KA, Chen L, Liu K, Chen X. Experimental study on mechanical properties of laminated bamboo beam-to-column connections. Eng Struct 2020;210:110305. https://doi.org/10.1016/j.engstruct.2020.110305.

[17] Li Z, He M, Tao D, Li M. Experimental buckling performance of scrimber composite columns under axial compression. Compos Part B Eng 2016;86:203–213. https://doi.org/10.1016/j.compositesb.2015.10.023.

[18] Li H, Su J, Xiong Z, Ashraf M, Corbi I, Corbi O. Evaluation on the ultimate bearing capacity for laminated bamboo lumber columns under eccentric compression. Structures 2020;28:1572–9. https://doi.org/10.1016/j.istruc.2020.10.004.

[19] Tinkler-Davies B, Shah DU. Digital image correlation analysis of laminated bamboo under transverse compression. Mater Lett 2021;283:128883. https://doi.org/10.1016/j.matlet.2020.128883.

[20] Zhou K, Li H, Hong C, Ashraf M, Sayed U, Lorenzo R, et al. Mechanical properties of large-scale parallel bamboo strand lumber under local compression. Constr Build Mater 2020:121572. https://doi.org/10.1016/j.conbuildmat.2020.121572.

[21] Li HT, Zhang QS, Huang DS, Deeks AJ. Compressive performance of laminated bamboo. Compos Part B Eng 2013;54:319–328. https://doi.org/10.1016/j.compositesb.2013.05.035.

[22] Li HT, Zhang QS, Wu G. Stress-strain model of side pressure laminated bamboo under compression. Journal of Southeast University 2015; 45: 1130-1134. DOI: 10.3969/j.ssn.1001-0505.2015.06.019.

[23] Sharma B, Gatóo A, Bock M, Ramage M. Engineered bamboo for structural applications. Constr Build Mater 2015;81:66–73. https://doi.org/10.1016/j.conbuildmat.2015.01.077.

[24] Yang D, Li H, Xiong Z, Mimendi L, Lorenzo R, Corbi I, et al. Mechanical properties of laminated bamboo under off-axis compression. Compos Part A Appl Sci Manuf 2020;138:106042. https://doi.org/10.1016/j.compositesa.2020.106042.

[25] Wei Y, Zhou M, Zhao K, Zhao K, Li G. Stress–strain relationship model of glulam bamboo under axial loading. Adv Compos Lett 2020;29:2633366X2095872. https://doi.org/10.1177/2633366x20958726.

[26] Luna P, Takeuchi C, Alvarado C, Moreno I. Glued laminated guadua angustifolia bamboo columns. Acta Hortic 2013;1003:125–30. https://doi.org/10.17660/ActaHortic.2013.1003.16.

[27] Xiao Y, Feng L, Lv XH, She LY, Shen YL. Experimental studies of GluBam columns under axial loads. Industrial Construction 2015; 45: 13-17. DOI: 10. 13204 /j.gyjz201504003.

[28] Li HT, Su JW, Zhang QS, Deeks AJ, Hui D. Mechanical performance of laminated bamboo column under axial compression. Compos Part B Eng 2015;79:374–3[3]82. https://doi.org/10.1016/j.compositesb.2015.04.027.

[29] Tian L min, Kou Y feng, Hao J ping. Axial compressive behaviour of sprayed composite mortar–original bamboo composite columns. Constr Build Mater 2019;215:726–7[4]36. https://doi.org/10.1016/j.conbuildmat.2019.04.234.

[30] Tan C, Li H, Wei D, Lorenzo R, Yuan C. Mechanical performance of parallel bamboo strand lumber columns under axial compression: Experimental and numerical investigation. Constr Build Mater 2020;231:117168. https://doi.org/10.1016/j.conbuildmat.2019.117168.

[31] Hong C, Li H, Xiong Z, Lorenzo R, Corbi I, Corbi O, et al. Review of connections for engineered bamboo structures. J Build Eng 2020;30:101324. https://doi.org/10.1016/j.jobe.2020.101324.

[32] Xiao Y, Shan B. GluBam structures. Beijing: China Architecture & Building Press; 2013.

[33] Tan C, Li H, Ashraf M, et al. Evaluation of axial capacity of engineered bamboo columns. Journal of Building Engineering 2021; 34: 102039. https://doi.org/10.1016/j.jobe.2020.102039.

[34] Washizu K. VARIATIONAL METHOS IN ELASTICITY AND PLASTICITY. International Series of Monographs in Aeronautics and Astronautics, 1968.

[35] Jasieńko J, Nowak T, Czepizak D. Numerical analysis of CFRP-reinforced wooden beams under bending. 11th World Conf Timber Eng 2010, WCTE 2010 2010;1:611–8.

[36] Tang G, Yin L, Li Z, Li Y, You L. Structural behaviors of bolted connections using laminated bamboo and

steel plates. Structures 2019; 20:324–39. https://doi.org/10.1016/j.istruc.2019.04.001.

[37] Hill R. A theory of the yielding and plastic flow of anisotropic metals. Proceedings Royal Society London A Mathematical, Physical Engineering Sciences 1948;193:281–97. https://doi.org/10.1098/rspa.1948.0045

[38] Saliklis EP, Falk RH. Correlating off-axis tension tests to shear modulus of wood-based panels. Journal of structural engineering 2000; 126: 621-625. https://doi.org/10.1061/(ASCE)0733-9445(2000)126:5(621)

[39] Ramirez F, Correal JF, Yamin LE, Atoche JC, Piscal CM. Dowel-Bearing Strength Behavior of Glued Laminated Guadua Bamboo . J Mater Civ Eng 2012; 24:1378–87. https://doi.org/10.1061/(asce)mt.1943-5533.0000515.